Theor Chem Acc (2011) 129:349–358
DOI 10.1007/s00214-010-0850-3

REGULAR ARTICLE

Calculated tautomeric equilibria and X-ray structures of 2-substituted N-methoxy-9-methyl-9H-purin-6-amines

Lise-Lotte Gundersen · Carl Henrik Görbitz · Liina Neier · Heidi Roggen · Toomas Tamm

Received: 23 August 2010 / Accepted: 30 October 2010 / Published online: 20 November 2010

Abstract Density Functional Theory calculations of nine 2-substituted N-methoxy-9-methyl-9H-purin-6-amines in the amino and imino tautomeric forms, as well as the complexes of the same with dimethyl sulfoxide (DMSO), were performed using two functionals (BP86 and B3LYP) and two basis sets (SV(P) and def2-TZVP). Solid-state structures of two of the compounds were obtained from single-crystal X-ray diffraction techniques. It was found that the inclusion of both an explicit hydrogen-bonding partner (DMSO) as well as continuum solvation effects, and vibrational corrections to energy, were necessary for qualitative and reasonable quantitative agreement with observed tautomeric ratios. The solution-optimized geometries and X-ray structures were found to be in good agreement. NMR spectroscopy confirmed the dependence of the tautomeric ratios on hydrogen-bonding abilities, in addition to the dipole moment of the solvent in question. Natural Bond Orbital charges on the N-7 nitrogen, as well as the tautomeric ratios were used to explain the observed reactivities of the compounds toward N-7 alkylation.

Dedicated to Professor Pekka Pyykkö on the occasion of his 70th birthday and published as part of the Pyykkö Festschrift Issue.

Electronic supplementary material The online version of this article (doi:10.1007/s00214-010-0850-3) contains supplementary material, which is available to authorized users.

L.-L. Gundersen · C. H. Görbitz · H. Roggen
Department of Chemistry,
University of Oslo, Oslo, Norway

L. Neier · T. Tamm (✉)
Department of Chemistry,
Tallinn University of Technology,
Tallinn, Estonia
e-mail: tamm@yki.ttu.ee

Keywords Density functional theory · Tautomeric equilibria · X-ray structures · Purinamines

1 Introduction

Agelasines and ageloximes are antimicrobial and cytotoxic 7,9-dialkylpurinium salts isolated from marine sponges (*Agelas* sp.). More than ten such natural products are currently known [1–9]. A general structure and some examples are shown in Fig. 1.

We have synthesized several agelasines and analogs and studied their biological activities, which include very interesting antineoplastic and antimicrobial properties, indicating that optimized compounds may have potential for treatment of certain neglected diseases like tuberculosis, malaria, and leishmaniasis [10–17]. Also worth mentioning is that agelasine D exhibits antifouling activity on *Balanus improvisus* cyprids, but neglectable toxicity toward the cyprids [18].

Synthesis of agelasines requires regioselective alkylation of an adenine derivative to give a 7,9-dialkylated adeninium salt. However, alkylation on 9-substituted adenines give mainly 1,9-dialkyl derivatives, and when 7-alkyladenines are reacted with alkyl halides, the second N-substituent is preferably introduced on N-3. Treatment of an N-alkoxy-9-methyl-9*H*-purin-6-amine **1** (Fig. 2) with alkylating agents gives, on the other hand, the desired alkylating pattern (Fig. 2, compounds **2**) [19]. Thus, agelasines and analogs **3** have generally been synthesized as depicted in Fig. 2. The reason why an N^6-alkoxy group is required for N-7 alkylation appears to be poorly understood. We found that the substrates in the N-7 alkylation, N-alkoxy-9-methyl-9*H*-purin-6-amines **1**, exist as a mixture of two tautomers; amino tautomers **1** and imino

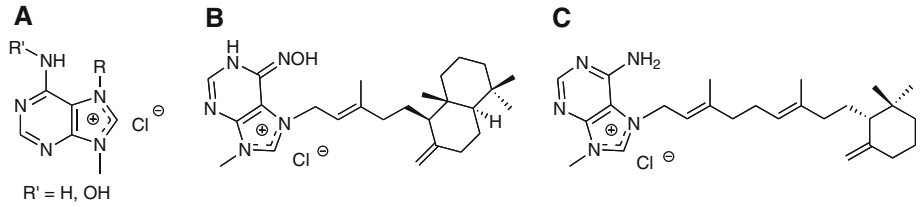

Fig. 1 General structure of agelasines (**a**, R′=H) and ageloximes (**a**, R′=OH), ageloxime D (**b**), and agelasine E (**c**)

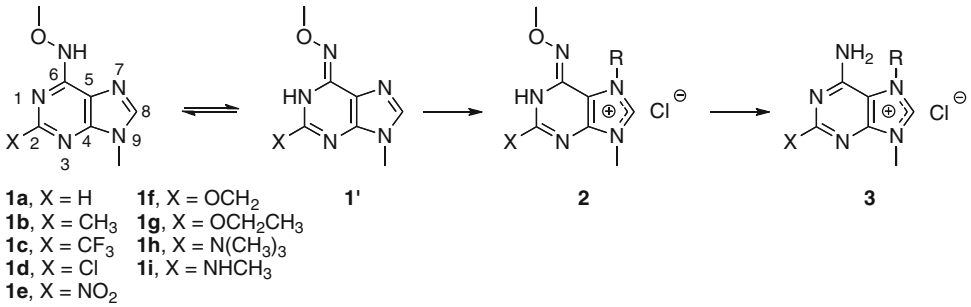

Fig. 2 General synthetic route to agelasines and analogs **3** and the structure of compounds **1a**–**i** studied herein. The numbering of the purine ring skeleton is shown on structure **1**

tautomers **1′** [11, 20]. The tautomeric ratio and the identity of each tautomer were determined by 1D and 2D ^{1}H, ^{13}C, and ^{15}N NMR spectroscopy techniques. To allow an imino structure, the NH must be situated in the purine 1-, 3- or 7-position. For the compound **1a** with X = H, the imino tautomer was established to have the NH hydrogen on N-1. For the compounds **1** where X ≠ H on the other hand, the placement of the NH could not be determined with certainty, but was assumed to be in the 1-position based on comparison of various shift values in particular C-4, C-6, N-1, and N^{6}, for the 2-substituted compounds **1b**–**1i** with the known 2-unsubstituted **1a**. Amino-imino tautomeric ratios were estimated in liquid solution (DMSO-d_6) from ^{1}H NMR data for all synthesized analogues **1a**–**1i**, as listed in Table 1 [20]. The amino tautomer was dominating for six compounds (**1c**–**1h**), while the equilibrium was shifted in favor of the imino form for the remaining three (**1a**, **1b,** and **1i**). We also found that the ratio between the tautomers, as well as the reactivity in the N-7 alkylation (synthesis of compounds **2**), is somehow related to the identity of the purine C-2 substituent (X in Fig. 2) [20]. To obtain more information on the structure and reactivity of compounds **1**, we decided to study the systems using computational chemistry and X-ray crystallography, in addition to the previously mentioned NMR spectroscopy [11, 20].

Accurate prediction of tautomeric ratios of biologically relevant compounds in solution is considered a challenge for the present-day quantum chemistry. The current state of the art of the field, as well as results of a blind test of the available methods, has been reviewed in a recent issue of the Journal of Computer-Aided Molecular Design. According to the overview presented therein [21], several of the current computational chemistry approaches are capable of predicting tautomeric energy differences with 5–10 kJ/mol accuracy. From among the methods described in this overview, ours is perhaps most similar to that of Klamt and Diedenhofen [22], but differs in some aspects: we use a simpler continuum solvation model, explicitly include a hydrogen bond acceptor, and do not include additional empirical corrections.

2 Results and discussion

2.1 Computations

Our approach to prediction of tautomeric equilibria is based on quantum-chemical computation of the corresponding energy differences between the relevant tautomeric forms. The energy of a tautomer in a given conformation is calculated as

$$E = E_{\mathrm{SCF+solv}} + E_{\mathrm{thermal}}$$

where $E_{\mathrm{SCF+solv}}$ is the total energy of the compound calculated with inclusion of the COSMO [23] solvation model as well as the outlying charge correction and E_{thermal} is the thermal contribution to enthalpy which includes the zero-point vibrational energy. The full enthalpy of the system would include an RT term, but since this is constant for all systems and we are only calculating energy differences between systems of identical chemical composition, it has been omitted. The calculated energy difference between the tautomers (ΔE) is used in the standard Boltzmann distribution formula to predict the tautomeric ratio that can be compared to the experimental values. For uniformity of treatment, all ratios are expressed as "percent amino tautomer" in this work.

Thorough conformational analysis of the systems was performed, and the lowest energy conformers selected for

Table 1 Calculated energy differences, and calculated and experimental tautomeric ratios of the compounds **1**

Compound	Substituent X	Single molecule						DMSO hydrogen-bonded complexes				NMR spectroscopy[a]
		BP86/SV(P)		BP86/def2-TZVP		B3LYP/def2-TZVP		BP86/def2-TZVP		B3LYP/def2-TZVP		
		ΔE, kJ/mol	% amino	ΔE, kJ/mol	% amino	ΔE, kJ/mol	% amino	ΔE, kJ/mol	% amino	ΔE, kJ/mol	% amino	% amino
1a	H	7.1	5	9.9	2	4.7	13	5.8	9	2.1	30	20
1b	CH_3	9.9	2	14.7	0	10.2	2	10.3	2	6.6	7	18
1c	CF_3	−7.8	96	−7.1	95	−14.3	100	−16.5	100	−21.7	100	100
1d	Cl	−8.3	97	−5.8	91	−10.8	99	−17.6	100	−21.9	100	100
1e	NO_2	−8.1	96	−5.6	90	−12.8	99	−23.5	100	−31.0	100	100
1f	OCH_3	2.4	*28*	3.6	*19*	0.8	*42*	−2.0	69	−4.5	86	92
1g	OCH_2CH_3	2.1	*30*	3.3	*21*	−0.3	53	−5.4	90	−7.9	96	94
1h	$N(CH_3)_2$	−2.8	76	3.3	*21*	−0.5	55	−4.9	88	−9.4	98	100
1i	$NHCH_3$	1.2	39	5.3	10	1.5	36	12.5	1	9.3	2	28

Qualitatively wrong predictions are in italic

[a] Taken from Ref. [20]; data obtained in DMSO-d_6 at 25 °C

each tautomer. All minima were checked with vibrational analysis both in the gas phase and in solution. Bulk solvation effects, with DMSO as the solvent, were taken into account via the COSMO continuum model. Details of the calculations are described in the "Experimental section".

2.2 Tautomeric ratios

Amino-imino tautomeric ratios were calculated with several DFT-based models in order to find the computationally least demanding approach that would be able to predict the observed tautomeric ratios of all the nine systems under study. As a minimum requirement, the correct dominating tautomer (amino or imino) should be predicted. A quantitative (even if approximate) prediction of tautomeric ratios was a secondary goal.

The initial DFT calculations, primarily aiming at creation of a list of minima on the potential energy surface, were performed at the BP86/SV(P) level. The first tautomeric ratios were calculated from the energies of the lowest-lying conformers and are presented in Table 1. While the qualitative agreement with observations (that is, whether the amino or imino form is dominating) is fair, the wrong tautomer is predicted for **1f** and **1g**. The quantitative predictions do not agree well with the experimental observations. As a general trend, the imino tautomers appear to be predicted too stable relative to the amino forms. This, in turn, leads to lower Boltzmann probabilities of the amino forms, relative to experimentally observed abundances.

In the hope of increasing accuracy of the predictions, all known local minima of the compounds were submitted to BP86/def2-TZVP geometry optimizations, and the lowest energy conformers at this level were used to recalculate the tautomeric ratios. The results are presented in Table 1. Quantitative agreement with the experimental values did not improve. To the contrary, the **1h** now emerges as an additional qualitatively incorrect prediction. At this level of theory, we also checked the necessity of inclusion of various components of energy: continuum solvation effects, zero-point vibrational energy, and thermal corrections to the total energy. It was found that omission of any of the components would decrease the accuracy of predictions, thus proving the importance of all the listed energy contributions. We also briefly tested the hypothesis that an alternative nitrogen site could be protonated in the imino tautomer. Protonation at N-3 and N-7, instead of the hitherto assumed N-1, was tested for the compound **1f**. These tautomers turned out to have higher energy (+46 kJ/mol for N-3 and +36 kJ/mol for N-7 at BP86/def2-TZVP level). We conclude that significant protonation at these sites is unlikely.

The third model that was tested was the B3LYP/def2-TZVP. The "B3LYP_gaussian" variety of the well-known functional, rather than the Turbomole default definition, was chosen solely due to its greater popularity. Only the lowest energy conformers as found in the previous study were used at this step, except for **1a** and **1b**, where the energy difference between the lowest conformers had been very small (1–2 kJ/mol) at previous level of theory. No changes in conformer ordering due to use of a different model were observed. The predicted tautomeric ratios are slightly improved over the BP86 results, but the **1f** remains qualitatively incorrect and the **1g** and **1h** are borderline cases where the energies of the two tautomers are predicted essentially equal, while experimentally the amino tautomer clearly dominates.

Next, we tested the hypothesis that hydrogen bonding to the solvent, DMSO, may be responsible for the discrepancy between the calculated and observed tautomeric ratios. NMR studies of the 2-ethoxy compound **1g** in various solvents indicated that hydrogen bonding between the compound in question and the solvent, but also the polarity of the solvent, is essential for the tautomeric ratio. As the dipole moment of the solvent increases, the amount of the amino tautomer also increases (Table 2). In addition to this general increase, the percent amino tautomer is much higher in solvents that can take part in hydrogen bonding compared with in those that cannot. Similar NMR studies of other compounds in the series proved problematic because of limited solubility in certain solvents.

As a computational counterpart to these experimental results, a molecule of DMSO at different orientations and locations was added to the lowest energy tautomers calculated previously, always oriented with either the oxygen or sulfur atom toward the proton relevant in the tautomerism. The initial geometries were submitted to the same computational procedures as described before. The BP86/def2-TZVP level was used for refinement of the relative orientation and position of the two molecules, and eradicating the transition states primarily due to rotation of the methyl group at N-9. Only the lowest energy geometries were re-calculated at the B3LYP/def2-TZVP level. The results are presented in Table 1. Sample geometries of some complexes are presented on Fig. 3.

Table 2 Percentage of amino tautomer **1g** present in different solvents

Solvent	Dipole moment[a] [24]	H-bond acceptor	% Amino[e]
Benzene-d_6	0.07[b]	–	13
$CDCl_3$	1.08[c]	–	24
CD_2Cl_2	1.59[c]	–	29
CD_3OD	1.67[c]	+	74
Acetone-d_6	2.78[c]	+	84
DMSO-d_6	3.94[d]	+	92

Taken from Ref. [24]

[a] For non-deuterated species

[b] liquid

[c] In benzene

[d] Gas

[e] Determined by ^{1}H NMR spectroscopy at 25 °C

The inclusion of an explicit hydrogen-bonded DMSO molecule appears to be significant in reaching quantitative agreement with the experimentally observed tautomeric ratios. Both of the functionals predict qualitatively correct dominating tautomer for all cases. The B3LYP results appear quantitatively more accurate, at the expense of at least threefold computational cost—the non-hybrid functional is easily paired with the Resolution of Identity approximation, while the B3LYP is not. We can conclude that inclusion of an explicit hydrogen-bonding partner leads to a satisfactory quantitative agreement between the predicted and calculated tautomeric ratios.

2.3 Molecular geometries

The purine ring system of the molecules is essentially planar. A flexible part common to all molecules **1** is the aminomethoxy group ($NOCH_3$) at C-6. Additional flexibility is possible in the substituent X at C-2, in addition to rotation of the methyl group at N-9 which is discussed in the "Experimental section".

Ignoring shallow local minima which may be artifacts of the computational model, the $-NOCH_3$ group at C-6 has two distinct minima on the rotational surface: the O–CH_3 part is directed either toward the N-1 (*syn*-configuration) or the N-7 (*anti*-configuration) (Fig. 4). Independent of the substituent X, the imino form always clearly prefers the *syn*-configuration, which may be rationalized by a hydrogen bond between the imino hydrogen at N-1 and the lone pairs of the oxygen of the side chain. The *anti*-orientation breaks this hydrogen bond and, consistent with typical hydrogen bond breaking energies, is 12–17 kJ/mol higher in energy. Also NMR [11, 25, 26] and UV [25] spectroscopical studies of the imine **1a′** and other 6-methoxyaminopurines indicate that the imines exist in the *syn*-configuration.

In the amino tautomer, N-1 is unprotonated, and the *syn* and *anti* orientations are close in energy. The differences between these two conformers are typically 2–5 kJ/mol, depending on the computational model and substituent X. In the gas phase model, the preferred orientations are in some cases reversed relative to the solution phase, again with differences smaller than 5 kJ/mol. Still, for all compounds **1** studied, the amino tautomers in solution phase consistently prefer the *syn* orientation of this side chain, even if by a very small margin.

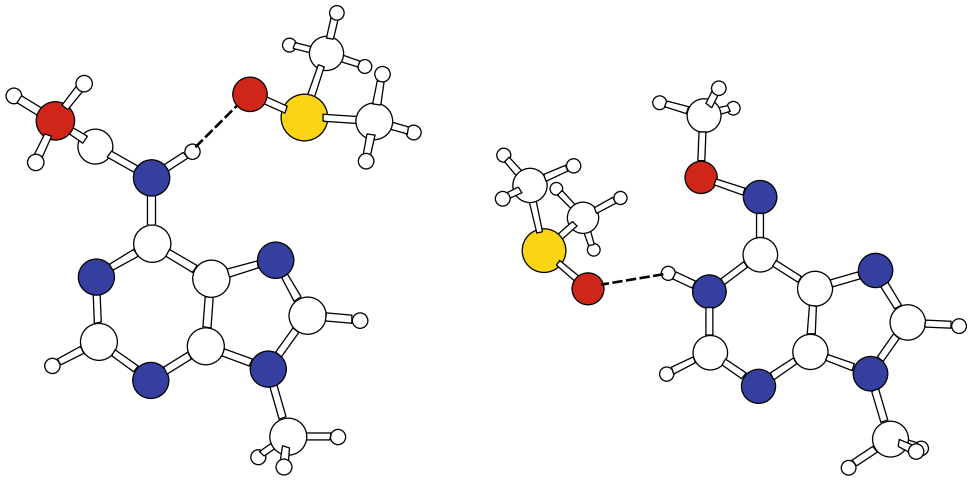

Fig. 3 Hydrogen-bonded complexes of **1a** and **1a**′ with a DMSO molecule

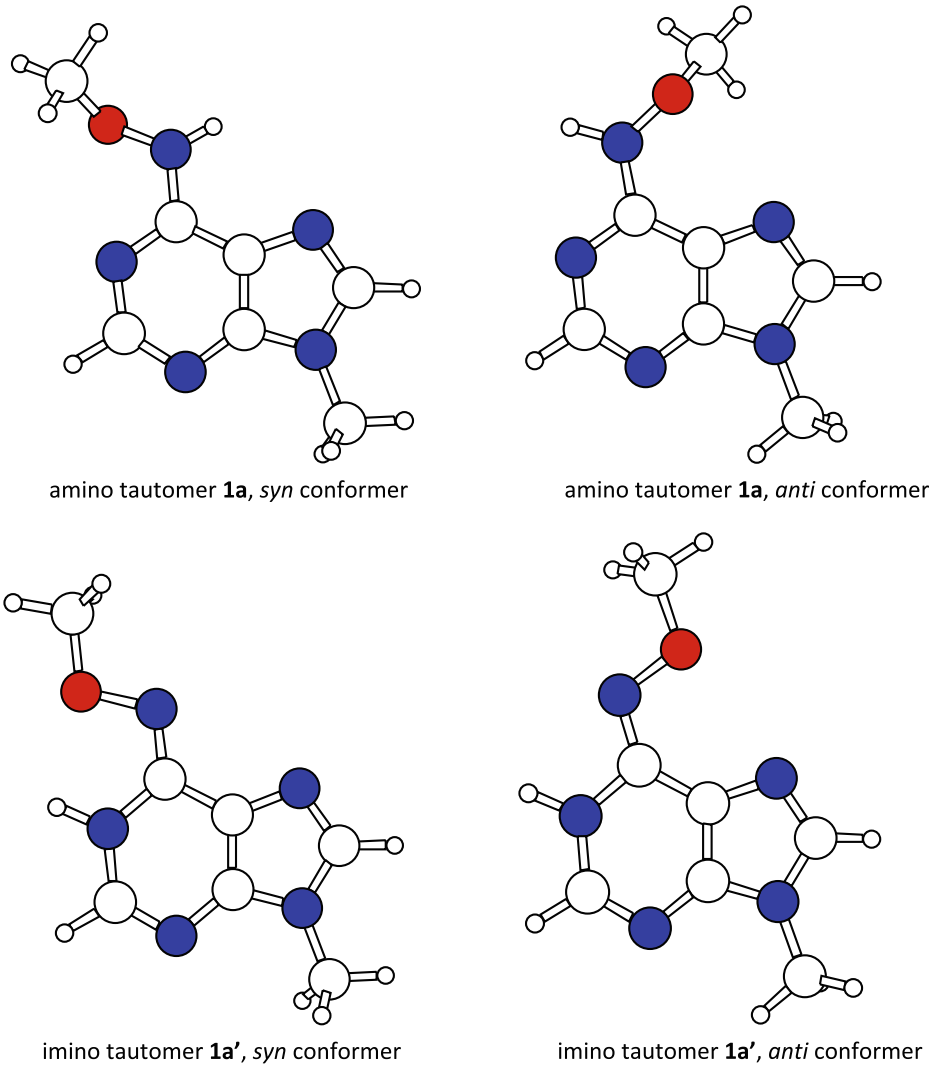

Fig. 4 Different orientations of the N–O–CH_3 side chain in compounds **1a** and **1a**′

Because the inclusion of explicit hydrogen bond acceptor increased the accuracy of energetic predictions, the lengths of the relevant N–H bonds were studied in order to see how the DMSO molecule affects the relevant nitrogen–hydrogen distances. At the B3LYP/def2-TZVP level, in the systems without explicit DMSO molecule, the

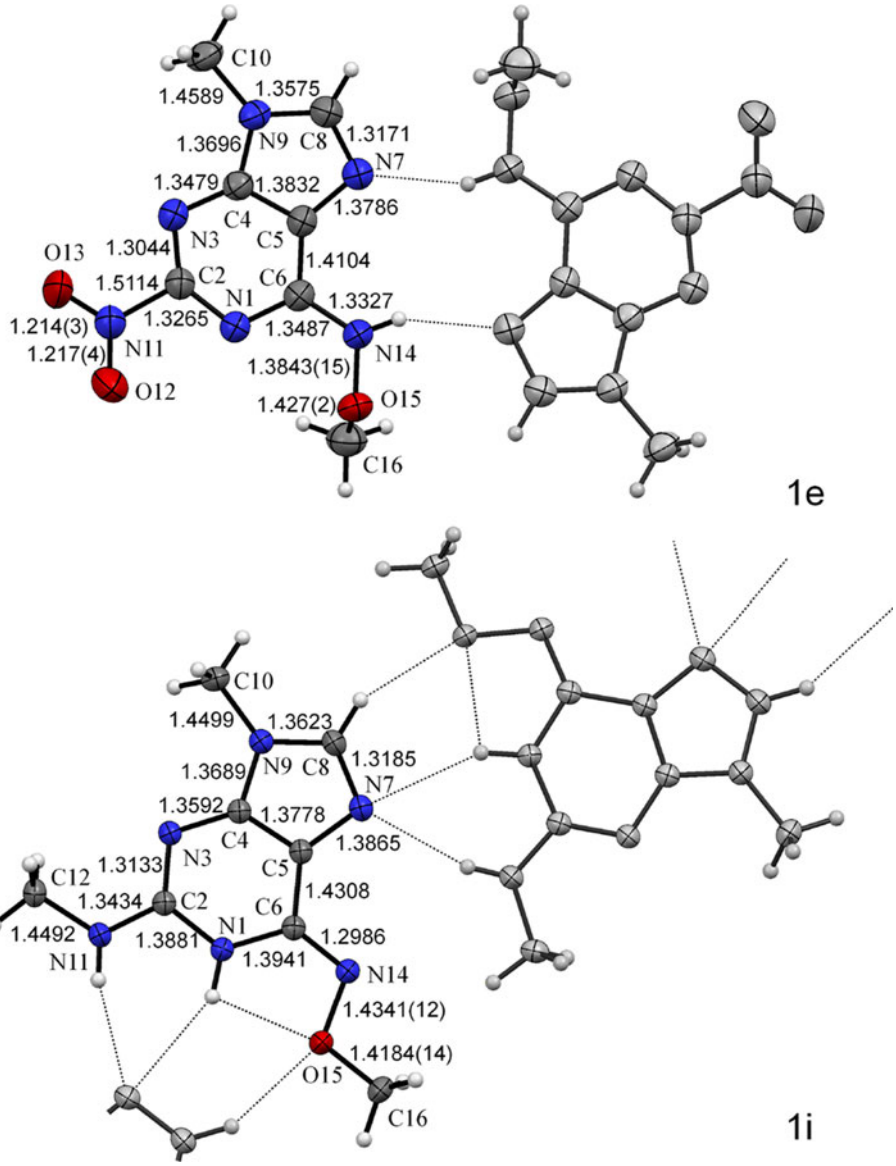

Fig. 5 Crystal structure of **1e** (*top*, $T = 296$ K) and **1i** (*bottom*, $T = 150$ K) with thermal ellipsoids drawn at the 50% probability level. **1e** forms hydrogen-bonded dimers, the partner molecule (symmetry code: $1 - X, -Y, 1 - Z$) is depicted in *gray color*. Adenine molecules in **1i** form one-dimensional ribbons, one full neighboring molecule (symmetry code: $-0.5 + X$, $0.5 - Y$, $-0.5 + Z$), and a group of three atoms of another molecule (symmetry code: $0.5 + X$, $0.5 - Y$, $0.5 + Z$) are included in *gray color*. Covalent bond lengths (in Å) are indicated. The estimated standard deviations (esds) bonds are given in parentheses for N–O and C–O bonds; for N–C and C–C bonds they are 0.0018 −0.0019 Å (**1e**) or 0.0014 Å (**1i**)

N–H distances were close to 1.01 Å, irrespective of the tautomer. There was almost no difference in the distance between the gas and solution phases, either. The inclusion of the hydrogen bond acceptor caused a slight lengthening of the bond distances, the average now being 1.03 Å for the amino forms and 1.02 Å for the imino forms. Surprisingly, however, the imino form of **1h** [X=N(CH_3)$_2$], which has the shortest N–H distance in the isolated molecule, does not experience a lengthening of the bond in the presence of the DMSO molecule either, the bond remaining at 1.008 Å.

The single-crystal structures of **1e** and **1i** are shown in Fig. 5. In agreement with previously acquired amino-imino tautomeric ratios in liquid solution (DMSO-d_6) [20] and current calculated ratios, **1e** has been crystallized as the amino tautomer, with formation of dimers located on inversion centers, while the imino form was obtained for **1i**. The extra hydrogen bond donor on N11 compared to **1e** enables **1i** to form extended hydrogen-bonded ribbons in the solid state. A complete set of hydrogen bond geometry parameters is available in the supplementary material.

The availability of experimental crystal structures makes direct comparison with the computed structural data possible. The main geometric parameters of **1e** at two different levels of theory, and the experimental values, are presented in Table 3. Both computational methods predict the geometry of the molecule with good accuracy. The mean absolute error for bond lengths is 0.011 Å for BP86/def2-TZVP and 0.008 Å for B3LYP/def2-TZVP. The former method tends to overestimate bond lengths (mean error 0.010 Å, only three of the 15 bonds are shorter than experiment), while the latter has more evenly distributed errors (mean error 0.002 Å). The *syn* orientation of the –N–O–CH_3 group is observed also in the experimental structures of both **1e** and **1i**. The agreement between the

Table 3 Calculated and experimental bond distances and angles of the amino form of **1e**

Parameter	*BP86/def2-TZVP*	*B3LYP/def2-TZVP*	Experiment
N1–C2, Å	1.3271	1.3190	1.3265(18)
C2–N3, Å	1.3241	1.3112	1.3044(18)
N3–C4, Å	1.3427	1.3369	1.3479(18)
C4–C5, Å	1.4087	1.3988	1.3832(19)
C5–C6, Å	1.4185	1.4096	1.4104(19)
C6–N1, Å	1.3479	1.3383	1.3487(17)
C4–N9, Å	1.3763	1.3676	1.3696(17)
N9–C8, Å	1.3733	1.3679	1.3575(19)
C8–N7, Å	1.3284	1.3158	1.3171(19)
N7–C5, Å	1.3756	1.3718	1.3786(17)
N9–C10, Å	1.4596	1.4580	1.4589(18)
C6–N14, Å	1.3606	1.3567	1.3327(18)
N14–O15, Å	1.3996	1.3912	1.3843(15)
O15–C16, Å	1.4471	1.4380	1.427(2)
C2–N11, Å	1.5146	1.5061	1.5114(18)
N1–C6–N14, deg	120.40	120.33	120.59(12)
C6–N14–O15, deg	118.42	118.33	120.78(12)
N14–O15–C16, deg	110.08	110.82	110.67(12)
N1–C6–N14–O15, deg	−21.65	−22.12	2.7(2)
C6–N14–O15–C16, deg	109.45	107.80	87.96(2)

The calculated values correspond to solution phase, while the experimental numbers are from solid state

Table 4 Calculated NBO atomic charges on N-7 in the tautomers **1** and **1′**, the field/inductive parameter (*F*) for the substituents X and isolated yield from N-7 benzylation of compounds **1**

Compound	Substituent X	*F*[a]	NBO charge on N-7 (amino tautomers)	NBO charge on N-7 (imino tautomers)	Yield of 2[b], %
1a	H	0.03	−0.481	−0.479	51
1b	CH_3	0.01	−0.483	−0.486	57
1c	CF_3	0.38	−0.477	−0.479	<2[c]
1d	Cl	0.42	−0.476	−0.479	4[d]
1e	NO_2	0.65	−0.473	−0.473	–
1g	OCH_2CH_3	0.26	−0.479	−0.485	52
1h	$N(CH_3)_2$	0.15	−0.487	−0.487	61
1i	$NHCH_3$	0.03	−0.483	−0.486	56

[a] Taken from Ref. [30]

[b] Taken from Ref. [20]

[c] Calculated from NMR

[d] Isolated as betaine

calculated geometric parameters of **1i** and the corresponding crystal structure is comparable to the agreement for **1e** (table available in the supplementary material).

2.4 Natural bond orbital analysis

As described above, when the field/inductive withdrawing abilities of the C-2 substituents in compounds **1** increase, the tautomeric ratio of **1** to **1′** is shifted toward **1**. Furthermore, we have previously observed that the reactivity of **1**/**1′** in N-7 alkylation is reduced (see Fig. 2, conversion of **1** to **2**) [20]. As the N-7 nitrogen of the purine ring system must function as the nucleophile in the alkylation of compounds **1**, a reduction in electron density may explain the reduction in reactivity at this site. An alternative explanation is that the reactivity is in some way directly affected by the tautomeric structure of the purine, with the imines being more reactive than the amines.

Hence, we performed a partial Natural Bond Orbital (NBO) analysis [27] (only calculation of atomic charges is implemented in Turbomole) of the electronic structures of **1a–i** and **1′a–i**. In Table 4, we have shown the calculated atomic charge on the N-7 in the amines **1a–i** as well as in the corresponding imines **1′** based on the B3LYP/def2-TZVP results in solution phase where hydrogen bonding is included, and the yields of N-7 benzylated product **2**. As the methoxy substrate **1f** is partially decomposed in the reaction, this analog is not included in the table or the following discussion. The reaction medium for the N-7 benzyations was dimethylacetamide (DMA). Although the same solvent was not used for calculations on the substrates and the reactions, both solvents in question may act

as hydrogen-bonding acceptors, and their dielectric permittivities are close (46 [28] for DMSO and 39 [29] for DMA), and their differences should not be essential for the current purpose. The results indicate that a minimum negative charge is required on N-7 for the alkylation to occur. If this negative charge is too low, poor yields are observed. Similar results are seen for the other computational model and also when no hydrogen bonding to a solvent molecule is included. However, it must be stressed that the charge differences found between the reactive and un-reactive substrates are small, and it could not be ruled out that also other factors not studied in here are important for reactivity.

3 Conclusions

Computations with the B3LYP hybrid functional and using a large basis set (def2-TZVP), inclusion of continuum solvent effects and an explicit hydrogen-bonding partner, and taking into account of vibrational and thermal contributions to energy are all necessary in order to achieve full qualitative and reasonable quantitative description of the tautomeric ratios of the title compounds. The computationally cheaper (using the RI approximation) BP86 functional delivers only slightly worse accuracy. Models without explicit hydrogen bond partner are qualitatively incorrect for several of the compounds studied.

Geometries of the calculated molecules are in good agreement with the X-ray results presented in the present work. The *syn* orientation of the aminomethoxy group is correctly predicted for the two compounds studied with the X-ray method.

The computational description helps to shed light on the experimental findings on the structure and chemical reactivity of the systems, depending on the substituent, X. As the field/inductive parameter of the substituent X increases, the electron density on N-7 is reduced and the tautomeric ratio of **1**/**1′** is shifted toward **1**. One or both of these effects may cause the following reduction in reactivity seen in N-7 alkylation.

4 Experimental section

4.1 NMR spectroscopy

^{1}H NMR spectra were recorded at 200 MHz with a Bruker avance DPX 200 instrument.

4.2 Details of computations

Standard Density Functional Theory methodology was used, with the functionals and basis sets as listed above. Geometries were fully optimized without constraints, except for occasional fixing of the rotation of the methyl group at N-9 as described below.

All molecules in this study have one or more conformationally flexible groups, and a conformational search was carried out in order to find the most stable conformers. Initial geometries of the conformer candidates were generated using a script that rotates the corresponding groups with a 90° step. Such a small step size was chosen in order to avoid missing any minima on the potential energy surface, which are expected to occur at approximately 120° separation. Indeed, additional shallow local minima were occasionally observed on the rotational surface of the –N–O–CH_3 group around the C–N axis in the solution phase. After refinement of the geometries at the BP86/SV(P) level both in gas phase and solution, the local minima were grouped by close values of energy and the relevant dihedral angles. The lowest energy conformer of each group was used for further studies.

Vibrational analysis of the obtained stationary points was always performed. In case of imaginary eigenvalues of the Hessian, the corresponding vibrational mode was visualized and geometry changed in order to obtain a true minimum on the potential energy surface. During this process, it was observed that the methyl group at N-9 has an extremely low barrier for rotation. A difference between energy maximum and minimum in the order of 1 J/mol (0.001 kJ/mol) was observed for several systems. At the default convergence criteria of the Turbomole package, the geometries often converged to a transition state along this rotational mode. Increasing the strictness of convergence criteria by 10 times both in the SCF procedure and in the geometry optimization, as well as using a denser ("m5") integration grid in the DFT step, usually led to a true minimum geometry. In a few cases, to reach a stationary point with all non-imaginary eigenvalues, we had to fix the dihedral angle of the N-9-methyl group at 10° intervals and performed constrained optimizations of such structures. The lowest energy structure with all non-imaginary eigenvalues was chosen for further work.

Bulk solvation effects were taken into account via the COSMO [23] continuum model. Default parameters, optimized atomic radii as defined in Turbomole, and the dielectric permittivity of 46 for DMSO were used.

The vibrational frequencies necessary for the E_{thermal} calculations were computed for the gas phase, using a gas phase optimized geometry of the same tautomer (and conformer) as was used for the solution phase calculation. Use of the gas-phase derived contributions to free energy avoids double counting of the terms related to change of free energy in the gas-phase to liquid transition.

All modelling was performed with the Turbomole [31, 32] package, version 5.10. The total energies in Hartree are available in the electronic supplementary

material. Final optimized geometries of the systems are available from the authors upon request.

4.3 X-ray crystallography

Compounds **1e** and **1i** were synthesized as described before [20], and crystals suitable for X-ray crystallography were obtained by storing the reaction mixture at 2–5 °C over night.

X-ray data collections with APEX2 [33] were carried out at ambient temperature for **1e** and at 150 K for **1i** with an Apex II single-crystal CCD-diffractometer and MoK_α radiation ($\lambda = 0.71069$ Å), using a $0.55 \times 0.46 \times 0.32$ mm block-shaped specimen for **1e** and a $0.65 \times 0.40 \times 0.22$ mm block-shaped specimen for **1i**. For both compounds, data integration and cell refinement was performed with SAINT-PLUS [34], with subsequent absorption correction by SADABS [35] and structure solution as well as least-squares refinement (on F^2) with SHELXTL [36]. Positional parameters were refined for the H atoms involved in strong hydrogen bonds, other H atoms were positioned with idealized geometry and C–H distances fixed to 0.98 (CH_3, **1i**), 0.96 (CH_3, **1e**), or 0.93 Å (CH, **1e**). Free rotation was permitted for the methyl groups. U_{iso} values were set to $1.2U_{eq}$ of the carrier atom (NH and CH) or $1.5U_{eq}$ (CH_3). The nitro group of **1e** has one major (shown in Fig. 5) and one minor position with occupancies 0.907(11) and 0.093(11), respectively. A common isotropic parameter was refined for the two O atoms of the minor nitro group orientation, while the associated N atom received the same set of anisotropic parameters as the corresponding N atom of the major orientation.

The solid-state structures of **1e** and **1i** determined by single-crystal X-ray diffraction have been deposited at the Cambridge Crystallographic Data Centre, deposition numbers are CCDC 789455 and CCDC 789456, respectively. Additional experimental details are available in the electronic supplementary material.

1e: $C_7H_8N_6O_3$, $M = 224.19$, triclinic, $P\bar{1}$, $a = 7.936(3)$ Å, $b = 8.159(3)$ Å, $c = 8.679(4)$ Å, $\alpha = 107.561(4)°$, $\beta = 90.460(4)°$, $\gamma = 115.571(4)°$, $Z = 2$, $N_{observed} = 1{,}824$, $R[F^2 > 2\sigma(F^2)] = 0.039$, $wR(F^2) = 0.112$, CCDC 789455.

1i: $C_8H_{12}N_6O$, $M = 208.24$, monoclinic, $P2_1/n$, $a = 7.6562(3)$ Å, $b = 10.7744(4)$ Å, $c = 11.7194(4)$ Å, $\beta = 94.194(1)°$, $Z = 4$, $N_{observed} = 2{,}621$, $R[F^2 > 2\sigma(F^2)] = 0.049$, $wR(F^2) = 0.149$, CCDC 789456.

Acknowledgments The Norwegian Research Council is greatly acknowledged for a PhD scholarship to H.R. (grant 171323/V30), as well as for partial financing of the Bruker Avance instrument used in this study. The authors are grateful to NordForsk (project "CRYSTENG") for networking and mobility support. The work of T.T. was supported by Estonian Science Foundation grant no. 8255.

References

1. Nakamura H, Wu H, Ohizumi Y, Hirata Y (1984) Tettrahedron Lett 25:2989–2992
2. Wu H, Nakamura H, Kobayashi J, Ohizumi Y, Hirata Y (1984) Tettrahedron Lett 25:3719–3722
3. Capon RJ, Faulkner DJ (1984) J Am Chem Soc 106:1819–1822
4. Wu H, Nakamura H, Kobayashi J, Kobayashi M, Ohizumi Y, Hirata Y (1986) Bull Chem Soc Jpn 59:2495–2504
5. Hattori T, Adachi K, Shizuri Y (1997) J Nat Prod 60:411–413
6. Fu X, Schmitz FJ, Tanner RS, Kelly-Borges M (1998) J Nat Prod 61:548–550
7. Iwagawa T, Kaneko M, Okamura H, Nakatani M, Van Soest RWM (1998) J Nat Prod 61:1310–1312
8. Appenzeller J, Mihci G, Martin M-T, Gallard J-F, Menou J-L, Boury-Esnault N, Hooper J, Petek S, Chevalley S, Valentin A, Zaparucha A, Al-Mourabit A, Debitus C (2008) J Nat Prod 71:1451–1454
9. Hertiani T, Edrada-Ebel R, Ortlepp S, van Soest RWM, de Voogd NJ, Wray V, Hentschel U, Kozytska S, Müller WEG, Proksch P (2010) Bioorg Med Chem 18:1297–1311
10. Utenova BT, Gundersen L-L (2004) Tettrahedron Lett 45:4233–4235
11. Bakkestuen AK, Gundersen L-L, Petersen D, Utenova BT, Vik A (2005) Org Biomol Chem 3:1025–1033
12. Vik A, Hedner E, Charnock C, Samuelsen O, Larsson R, Gundersen L-L, Bohlin L (2006) J Nat Prod 69:381–386
13. Vik A, Hedner E, Charnock C, Tangen LW, Samuelsen O, Larsson R, Bohlin L, Gundersen L-L (2007) Bioorg Med Chem 15:4016–4037
14. Proszenyak A, Charnock C, Hedner E, Larsson R, Bohlin L, Gundersen L-L (2007) Arch Pharm (Weinheim, Ger) 340:625–634
15. Proszenyak A, Brændvang M, Charnock C, Gundersen L-L (2009) Tetrahedron 65:194–199
16. Vik A, Proszenyak A, Vermeersch M, Cos P, Maes L, Gundersen L-L (2009) Molecules 14:279–288
17. Roggen H, Charnock C, Burman R, Felth J, Larsson R, Bohlin L, Gundersen L-L (in Press) Arch Pharm (Weinheim, Ger)
18. Sjögren M, Dahlström M, Hedner E, Jonsson PR, Vik A, Gundersen L-L, Bohlin L (2008) Biofouling 24:251–258
19. Fujii T, Itaya T (1999) Heterocycles 51:393–454
20. Roggen H, Gundersen L-L (2008) Eur J Org Chem 5099–5106
21. Geballe MT, Skillman AG, Nicholls A, Guthrie JP, Taylor PJ (2010) J Comput Aided Mol Des 24:259–279
22. Klamt A, Diedenhofen M (2010) J Comput Aided Mol Des 24:621–625
23. Klamt A, Schüürmann G (1993) J Chem Soc B 799–805
24. McClellan AL (1974) Tables of experimental dipole moments, vol 2. Rahara Enterprises, El Cerrito
25. Fujii T, Saito T, Itaya T, Kizu K, Kumazawa Y, Nakajima S (1987) Chem Pharm Bull 35:4482–4493
26. Hill F, Williams DM, Loakes D, Brown DM (1998) Nucleic Acids Res 26:1144–1149
27. Reed AE, Weinstock RB, Weinhold F (1985) J Chem Phys 83:735–746
28. Riddick JA, Bunger WB, Sakano TK (1986) Organic solvents: physical properties and methods of purification. Wiley, New York
29. Świergiel J, Jadżyn J (2009) J Chem Eng Data 54:2296–2300
30. Hansch C, Leo A, Taft RW (1991) Chem Rev 91:165–195
31. Ahlrichs R, Bär M, Häser M, Horn H, Kölmel C (1989) Chem Phys Lett 162:165–169

32. Ahlrichs R, Arnim MV (1995) In: Chementi E, Cornigiu G (eds) Methods and techniques in computational chemistry: Metecc-95. STEF, Cagliari, pp 509–554
33. APEX2 (2007) Bruker AXS Inc., Madison, Wisconsin, USA
34. SAINTPLUS (2007) Bruker AXS Inc., Madison, Wisconsin, USA
35. SADABS (2007) Bruker AXS Inc., Madison, Wisconsin, USA
36. Sheldrick GM (2008) Acta Crystallogr Sect A Found Crystallogr 64:112–122